Removing speckle noise from the signals of a laser Doppler vibrometer on moving platforms (LDVom) by ensemble empirical mode decomposition

Jin, Yang; Dollevoet, Rolf; Li, Zili

DOI
10.1088/1361-6501/ac8daf

Publication date
2022

Document Version
Final published version

Published in
Measurement Science and Technology

PAPER • **OPEN ACCESS**

Removing speckle noise from the signals of a laser Doppler vibrometer on moving platforms (LDVom) by ensemble empirical mode decomposition

To cite this article: Yang Jin *et al* 2022 *Meas. Sci. Technol.* **33** 125205

OPEN ACCESS
IOP Publishing
Measurement Science and Technology
Meas. Sci. Technol. **33** (2022) 125205 (17pp)
https://doi.org/10.1088/1361-6501/ac8daf

Removing speckle noise from the signals of a laser Doppler vibrometer on moving platforms (LDVom) by ensemble empirical mode decomposition

Yang Jin, Rolf Dollevoet and Zili Li*

Railway Engineering, Delft University of Technology, Delft, The Netherlands

E-mail: Z.Li@tudelft.nl

Received 8 February 2022, revised 7 August 2022
Accepted for publication 30 August 2022
Published 15 September 2022

Abstract

With increasing requirements for structural stability and durability, effective monitoring strategies for existing and potential damage are necessary. A laser Doppler vibrometer on moving platforms (LDVom) can remotely capture large-scale structural vibrations, but speckle noise, a significant signal issue mainly when one-way continuously scanning from moving platforms, restricts its applications. A novel approach based on ensemble empirical mode decomposition (EEMD) is proposed to eliminate speckle noise. Moving root-mean-square thresholds are used to cut off signal drop-outs. With both numerically simulated and experimentally acquired signals, the proposed EEMD-based approach reveals the true vibrations despite the low initial signal-to-noise ratio. Other methods fail to eliminate the speckle noise. In physical experiments, the despeckled signal energy is concentrated at defect locations in the Hilbert–Huang spectrum. The identified damage locations agree well with the actual damage locations. Therefore, the developed approach demonstrates advantages and robustness of eliminating speckle noise in LDVom signals for damage inspection.

Keywords: laser Doppler vibrometer, speckle noise, noise removal, ensemble empirical mode decomposition

(Some figures may appear in colour only in the online journal)

1. Introduction

Structures deteriorate owing to mechanical loading and the consequent damage [1]. Although the evolution of materials [2] and construction technologies [3] has improved durability, long-term fatigue inevitably results in material defects threatening safe operation [4]. Therefore, an effective monitoring strategy is necessary for discovering damage, especially in the early stages. Modal analysis of structures under excitation is extensively applied to characterize the damage [5, 6], promoting the development of the needed instruments. Mainstream contact-measurement techniques, including contact sensors and ultrasound detectors, have been successful in scientific research and industrial applications [7, 8], but the drawbacks of adding unnecessary masses and thus possibly changing

* Author to whom any correspondence should be addressed.

Table 1. Comparison between different LDV measurement techniques.

LDV technique	Measurement strategy	Excitation source	Noise level	De-noise approach
Single-point	Single-point	No requirement	Weak	No need
SLDV	Pointwise	Cyclical	Weak	No need
CSLDV	Cyclical continuous scan	Cyclical	Medium	Energy-based, averaging, polishing surface
LDVom	One-way continuous scan	No requirement	Intense	Not applicable

modes have aroused numerous concerns. In addition, the contact sensors are inconvenient for measuring locations that are difficult to reach and scanning very long structures such as railway tracks at high speed. Therefore, noncontact technologies for acquiring vibration signals have been the subject of recent research.

A laser Doppler vibrometer (LDV) is a noncontact and nondestructive instrument for capturing the vibration velocity of object surfaces [9]. This instrument is based on Doppler effect, as the target vibration results in a frequency shift between the emitted and reflected laser beams [10]. It is worth noting that an LDV is appropriate for high-frequency and high-precision analysis, as its measuring frequency can be over 1 GHz and the geometric resolution of the vibration velocity can reach 1 mm s^{-1}. Recently, the LDV measurement systems have been demonstrated to be effective in laboratory experiments for vibration analysis (e.g. [11, 12]). However, the researches hardly applied LDV systems in monitoring large-scale structures, e.g. railway tracks, owing to the limitations of measurement techniques and signal quality [10, 13].

Major LDV measurement techniques includes a single-point LDV, a scanning LDV (SLDV), and a continuous SLDV (CSLDV), which are summarized in [10], but these techniques are not suitable for large-scale measurement. A single-point LDV [14] only acquires vibrations at one point, and the setup should move when measuring another point. The SLDV measurement [15–18] is an ensemble of single-point measurements with the setup simplified by rotating mirrors. However, it requires long-time acquisition at each point, which is time-consuming. A CSLDV continuously scans the vibrating surface, but it requires multiple reciprocating or cyclical scans for modal analysis [19–23]. In addition, SLDV and CSLDV need cyclical excitation, and thus the mode would not change during measurement. However, reciprocating or cyclical scans and cyclical artificial excitation cannot be realized in large-scale measurements. In contrast, an LDV on moving platforms (LDVom) [24] can one-way continuously scan the sample surface, especially those long structures like railway tracks. This technique is totally different from the previous ones (compared in table 1) and provides the possibility for large-scale measurements. However, improving signal quality becomes a primary task for the LDVom [24].

Speckle noise is a significant issue polluting the signals, which should be a priority in signal processing [10, 13, 25]. This noise is physically generated by the variation of laser speckle patterns, as introduced in section 2.1. Therefore, the variation rate affected by measurement techniques and the laser speckle patterns affected by laser wavelength and surface roughness [26] are the all influencing factors of speckle noise. This is not a noise generated by the instrumental units but by the laser beams [27]. For the single-point LDV or SLDV, speckle noise is extremely weak [9] since the variation rate of laser speckle patterns is nearly 0. In CSLDV measurements, the noise level increases, but the noise becomes pseudo-random since the signal spectrum consists of harmonic sidebands centering at the vibration frequency and spacing by the scanning frequency [10, 25]. Some strategies, such as the energy-based approaches [28], a scanning-average method [29], and polishing the vibrating surface [30], are effective in mitigating CSLDV speckle noise.

However, the aforementioned strategies are unsuitable to handle LDVom speckle noise: (a) with one-way measurement, the time series becomes crucial in addition to the energy spectrum. This is because only one measuring sample containing the vibration amplitude and phase at each point is acquired; (b) the scanning-average method can only be used to handle cyclical measurements like the CSLDV. LDVom signals cannot be averaged since the signals only contain the instantaneous vibration at each measuring point; (c) polishing the vibrating surface is unsuitable in large-scale measurement (e.g. the railway tracks over 1000 km). Besides, in physical experiments, the noise amplitudes can exceed 30 times that of the true vibration, and the signal-to-noise ratio (SNR) can drop below −15 dB [31]. To handle the severe noise and improve the signal quality, an effective approach for removing LDVom speckle noise remains to be found.

Empirical mode decomposition (EMD) is a self-adaptive approach proposed by Huang *et al* [32] for nonlinear and non-stationary signal analysis. It decomposes signals into multiple intrinsic mode functions (IMFs) containing instantaneous frequency information, and thus, the corresponding Hilbert transform has physical meaning. Differing from the wavelet transform and bandpass filters (BPFs) with certain bandwidths, the bandwidth of EMD is naturally determined by the signal itself. Since IMFs correspond to local modal responses, the decomposition results and Hilbert–Huang spectrum can highlight the abnormal local modes for defect inspection [33, 34]. In addition, EMD has the potential to eliminate distortions by noise and to preserve the actual oscillations, since each IMF presents continuity of the instantaneous frequencies. Numerous studies have developed EMD-based approaches for eliminating the environmental and instrumental noise of, e.g. lidar signals [35], electrocardiography signals [36] and seismic signals [37]. Nonetheless, speckle noise is much more complicated, as

frequent signal drop-outs exceed multiple times normal amplitudes and dominant noise components continuously distort actual oscillations. To the best of our knowledge, no research has utilized EMD for LDV speckle noise removal. Mode mixing is a significant issue affecting IMF components when applying EMD, and thus Wu and Huang [38] developed ensemble EMD (EEMD) assisted by white noise to address this problem.

In this paper, we propose an EEMD-based approach for speckle noise removal in LDVom signals. The despeckling effect is evaluated in both numerically synthesized and experimentally acquired signals. The remainder of this paper is organized as follows: section 2 introduces the LDV system and the despeckling algorithm; section 3 investigates the applicability of the developed approach in simulated signal analysis; section 4 analyzes the experimentally acquired signals for defect inspection; and section 5 discusses and concludes this paper.

2. Methodology

2.1. Speckle noise and its simulation

Speckle noise, or 'pseudo vibration' [39], is LDV measurement noise produced by an optical phenomenon called speckle patterns. When an optically rough surface is illuminated by a coherent laser beam, the incident wavelets are reflected in diverse directions; thus, their phases vary according to the surface deviations. The wavelets of the scattered laser interfere destructively or constructively, generating disorderly distributed dark-bright spots, namely, speckle patterns. Since the LDV photodetector focuses on the spot portion of the object surface, the signal output is generally the phasor summation of the interfered laser wavelets. When scanning from moving frames, the translation and deformation of the focusing spot result in significant speckle noise, as the light intensities and phases are dramatically altered over the variant speckle patterns. Specifically, signal drop-outs are extreme speckle noise produced by sharply varying speckle patterns.

The detected intensity, I, acquired by the photodetector is the combination of transmission and reference laser beams, and it can be expressed as [40]

$$I = I_{\mathrm{R}} + I_{\mathrm{T}} + 2\sqrt{I_{\mathrm{R}} I_{\mathrm{T}}}\cos\left[2\pi f_{\mathrm{R}} t - \frac{4\pi}{\lambda}\int v\,dt + (\varphi_{\mathrm{R}} - \varphi_{\mathrm{T}})\right] \tag{1}$$

where, I_{T} & I_{R} are intensities of the transmission and reference beams respectively, f_{R} is the frequency shift of the reference beam, λ is the laser wavelength, v is the vibration velocity of the targeted surface, and φ_{T} & φ_{R} are the phases of the transmission and reference beams respectively. According to equation (1), the beat frequency that the LDV system acquires is

$$f_{\mathrm{beat}} = f_{\mathrm{R}} - \frac{2}{\lambda}v + \frac{1}{2\pi}\frac{d(\varphi_{\mathrm{R}} - \varphi_{\mathrm{T}})}{dt}. \tag{2}$$

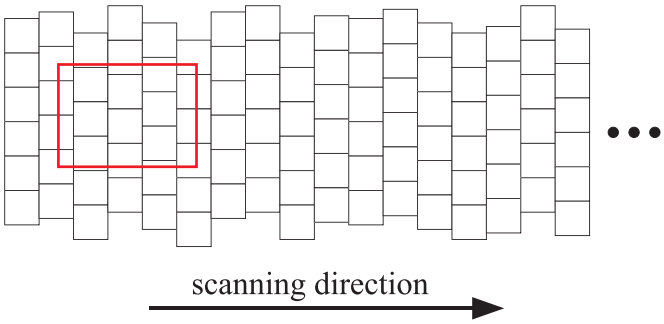

Figure 1. Speckle elements discretizing the object surface, as well as the photodetector along the scanning direction.

Considering the focusing spot A illuminated by the transmission beam with P wavelets (each with the phase ϕ_{Tp} and intensity I_{Tp}) and the reference beam with Q wavelets (each with the phase ϕ_{Rq} and intensity I_{Rq}), the resultant intensities and phases of speckles can be calculated by the following equations [27]:

$$I_{\mathrm{res}} = 2\sqrt{I_{\mathrm{R}} I_{\mathrm{T}}} = \frac{1}{A}\left\{\left[\sum_{q=1}^{Q}\sum_{p=1}^{P} A_{pq}\sqrt{I_{Rq} I_{Tp}}\sin(\phi_{Rq} - \phi_{Tp})\right]^2 + \left[\sum_{q=1}^{Q}\sum_{p=1}^{P} A_{pq}\sqrt{I_{Rq} I_{Tp}}\cos(\phi_{Rq} - \phi_{Tp})\right]^2\right\}^{1/2} \tag{3}$$

$$\tan\phi_{\mathrm{res}} = \tan(\varphi_{\mathrm{R}} - \varphi_{\mathrm{T}}) = \frac{\sum_{q=1}^{Q}\sum_{p=1}^{P} A_{pq}\sqrt{I_{Rq} I_{Tp}}\sin(\phi_{Rq} - \phi_{Tp})}{\sum_{q=1}^{Q}\sum_{p=1}^{P} A_{pq}\sqrt{I_{Rq} I_{Tp}}\cos(\phi_{Rq} - \phi_{Tp})} \tag{4}$$

where, I_{res} & ϕ_{res} are the time-varying resultant intensity and phase of the Doppler signal respectively, and the area A_{pq} overlaps the pth transmission wavelet and the qth reference wavelet. For the modulated Doppler signal, the measured velocity V_m becomes the combination of the actual vibration velocity v and the phasor variation (speckle noise).

$$V_m = \frac{\lambda}{2}(f_{\mathrm{R}} - f_{\mathrm{beat}}) = v - \frac{\lambda}{4\pi}\frac{d(\varphi_{\mathrm{R}} - \varphi_{\mathrm{T}})}{dt}. \tag{5}$$

According to equations (4) and (5), significant changes in ϕ_{res} can result in large velocity distortion, and the noise is basically produced by the intensity and phase distributions of speckle patterns. Considering these optical factors as stochastic variables, Rothberg [27] developed an approach for numerically simulating speckle noise that presented good agreement with experimental results.

Rothberg [27] assumed that speckles are rectangular and densely distributed, and divided the scanning surface into unaligned speckles, as shown in figure 1. These

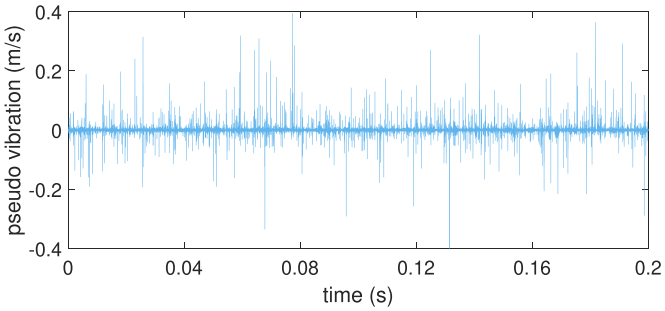

Figure 2. Simulated 0.2 s speckle noise with a sampling frequency of 102 400 Hz.

speckles are assigned different intensities and phases. The intensities satisfy a negative exponential probability distribution (equation (6)) and the phases are generated using a series of random numbers in the range of 0–2π [26, 27].

$$I_{Tp} = -\bar{I}\ln\left[1 - \frac{x_p}{1+(10^{-10})}\right] \tag{6}$$

where $\bar{I}$ is the mean intensity and x_p is a random number satisfying $0 \leqslant x_p \leqslant 1$.

The photodetector (the red rectangle in figure 1) focuses on the scanning surface to acquire the transmission beam reflected from an area of $m_0 \times n_0$ speckle elements, and the focusing position moves along the scanning direction. The size of each speckle element is $40 \times 40\ \mu m^2$ in this paper. Since only fractions of some speckles are inside the photodetector, the overlapping area A_{pq} is calculated for each speckle. The contribution of the reference beam can be simulated as a stationary speckle pattern with a certain intensity and phase. As the properties of both transmission and reference beams are defined, the speckle noise polluting the actual vibration can be determined by equations (3)–(5). Figure 2 illustrates simulated speckle noise with a sampling frequency of 102 400 Hz.

2.2. EEMD and the Hilbert–Huang spectrum

The EMD approach was originally proposed by Huang *et al* [32] to self-adaptively decompose signals within natural bandwidths. Since numerous systems are nonlinear and nonstationary, the instantaneous frequency in the IMFs and Hilbert–Huang spectrum contains more physical meaning than the Fourier frequency spectrum. The LDV scanning signal represents the instantaneous vibration velocity, whose characteristics can be analyzed by the IMFs. Specific definitions were developed to acquire ideal IMFs: for an IMF, (a) the number difference between extrema and zero-cross points should be no more than 1 and (b) the envelopes determined by the extrema should on average be 0. The EMD algorithm is described as follows:

Algorithm 1. Pseudo codes of EMD.

Input: original signal $v(t)$, maximum number of IMFs N_f, and the decomposition threshold SD;
$r_1 = v(t)$;
for $k = 1; k \leqslant N_f; k = k + 1$ **do**
  $h_{k,1} = r_k$;
  for $j = 1; j = j + 1$ **do**
    Find the upper and lower envelopes (U_j, L_j);
    $m_j = (U_j + L_j)/2$;
    Remove the envelope mean from the residual signal
    $h_{k,j+1} = h_{k,j} - m_j$;
    Stop when $\sum_{k=1}^{j} \frac{m_k^2}{h_{i,j}^2} < SD$;
  end
  $C_k(t) = h_{k,j+1} r_{k+1}(t) = r_k(t) - C_k(t)$
end
Ouput: the kth IMF $C_k(t)$ $(k = 1, 2, \ldots)$ and the residual $r_{N_f+1}(t)$

However, the significant issue of mode mixing, as more than one oscillation appears in the local waveform of IMFs, has aroused research concerns. A white-noise-assisted decomposition approach, namely EEMD, was developed by Wu and Huang [38] to handle this issue. The EEMD algorithm is summarized as follows [38]:

Algorithm 2. Pseudo codes of EEMD.

Input: original signal $v(t)$, maximum number of IMFs N_f, trials number n, and standard deviation of added noise σ_w;
for $k = 1; k \leqslant n; k = k + 1$ **do**
  Generate random Gaussian white noise $\text{noise}_k(t)$ with the standard deviation σ_w;
  $v'(t) = v(t) + \text{noise}_k(t)$;
  Decompose $v'(t)$ by EMD [32] to obtain the ith IMFs $C_{k,i}(t)$ and residual $r_k(t)$;
end
$C_i(t) = \sum_{k=1}^{n} C_{k,i}(t)/n$;
$r(t) = \sum_{k=1}^{n} r_k(t)/n$;
Ouput: the final ith IMF $C_i(t)$ $(i = 1, 2, \ldots)$ and the ultimate residual $r(t)$

To effectively apply EEMD in signal analysis, it is significant to determine the standard deviation σ_w of added noise and the trials number n of EMD. As mentioned in [33, 38], setting σ_w to 0.2 times the standard deviation of the original signal and n to several hundred is a good practice.

The Hilbert transform considers the signal as the projection of a spiral curve and calculates the complex conjugate pair of the signal. With the specific definitions, the Hilbert transform of any IMF has physical meanings that can be expressed as [32]

$$C_i'(t) = \frac{1}{\pi} P_c \int_{-\infty}^{\infty} \frac{C_i(\tau)}{t-\tau} d\tau \tag{7}$$

where, P_c is the Cauchy principal value and $C_i(\tau)$ represents any IMF. Therefore, the analytical signal of any IMF can be expressed as

$$Z_i(t) = C_i(t) + \mathbf{j}C_i'(t) = a_i(t)e^{\mathbf{j}\theta_i(t)} \tag{8}$$

where, $a_i(t) = \sqrt{C_i^2(t) + C_i'^2(t)}$ is the signal amplitude, $\theta_i(t) = \arctan(\frac{C_i'(t)}{C_i(t)})$ is the signal phase, and **j** represents the imaginary unit. Through the application of the Hilbert transform to all IMFs, the analytical signal of the original data can be obtained [32].

$$Y(t) = \sum_{i=1}^{N_f} a_i(t)e^{\mathbf{j}\int \omega_i(t)dt} \tag{9}$$

where $\omega_i(t)$ represents the instantaneous frequency. Therefore, the analytical amplitudes are represented as functions of instantaneous frequency and time, and the Hilbert–Huang spectrum can be illustrated simply as amplitudes in the frequency-time domain. Indeed, the amplitude in an IMF corresponds to the operating deflection shape inside a specific frequency band, and thus the Hilbert–Huang spectrum has potential for vibration analysis using the LDVom signals.

2.3. Proposed despeckling algorithm

As the amplitudes of signal drop-outs are considerably larger than the actual vibration, they dramatically can distort local waveforms. The moving root-mean-square (MRMS) thresholds are used for cutting off the outliers to reduce this effect.

$$T_u(t) = M(t) + 2\sqrt{\frac{v^2(t) \bigotimes e_N}{N}}$$

$$T_l(t) = M(t) - 2\sqrt{\frac{v^2(t) \bigotimes e_N}{N}} \tag{10}$$

where, $T_u(t)$ & $T_l(t)$ are upper and lower thresholds respectively; $M(t)$ is the moving signal average; $v(t)$ is the original signal; $\bigotimes$ represents the convolution calculation; N is the window length of MRMS; and e_N is the all-one vector with length N. Hence, the signal amplitudes outside the thresholds are replaced by values on the thresholds. This procedure has two potential effects, reducing drop-out amplitudes and generating oscillation discontinuities that represent noise locations.

The following is the algorithm developed in this paper for eliminating speckle noise:

Algorithm 3. Removing speckle noise

Input: original signal $v(t)$;
1. Apply MRMS thresholds to cut off signal drop-outs and obtain $y_0(t)$;
2. Decompose $y_0(t)$ by EEMD and obtain all IMFs $C_i(t)$ and the residual $r(t)$;
3. Discard the first few IMFs related to noise;
4. Calculate the despeckled signal $V(t)$ by summing the remaining IMFs and the residual;
Ouput: despeckled signal $V(t)$

3. Simulated signal analysis

3.1. Simulated signal construction

Three simulated signals polluted by speckle noise with different signal-to-noise ratios (SNRs) are constructed hereafter to evaluate the despeckling effects. All simulated signals are sampled at frequencies of f_s =102 400 Hz.

The first signal $v_1(t)$ consists of two harmonic vibrations and randomly simulated speckle noise. A multiplication parameter ρ is utilized to adjust the SNR. Figure 3 illustrates the polluted signal with SNR $= -10$ dB (usually, SNR < 0 in practical cases). The actual vibration component is almost invisible in figure 3(a), and the noise dramatically distorts the waveforms in the magnified signal (figure 3(b)).

$$v_1(t) = 0.005[\cos(2\pi \times 2000t) + \sin(2\pi \times 1200t)] + \rho \cdot \text{noise}. \tag{11}$$

The signal $v_2(t)$ is produced by adding speckle noise to the data taken from [41]. Figure 4 presents the polluted signals with SNR $= -10$ dB. Similar to the signal $v_1(t)$, the speckle noise dramatically distorts the actual waveforms.

$$v_2(t) = \frac{1}{200(1.2 + \cos(100\pi t))} + \frac{\cos(160\pi t + 0.2\cos(320\pi t))}{200(1.5 + \sin(100\pi t))} + \rho \cdot \text{noise}. \tag{12}$$

The signal $v_3(t)$ is produced by adding speckle noise to the data taken from [42]. This signal is an unusual one without physical meanings. We only evaluate the despeckle effect on this signal. figure 5(a) presents the polluted signals with SNR $= -10$ dB.

$$v_3(t) = v_{3a}(t) + \rho \cdot \text{noise}. \tag{13}$$

3.2. Despeckling results

Two criteria, the SNR after despeckling processing and correlation coefficient δ (equation (14)) between the actual vibrations and despeckled signals, are used to evaluate the developed approach. Three different noise conditions with initial SNR $= -10$ dB, -5 dB & -15 dB are considered by modifying the parameter ρ. Other signal processing approaches including the BPF [43] and the discrete wavelet transform (DWT) [44] are utilized for comparison.

$$\delta(v, v_a) = \frac{\text{Cov}(v, v_a)}{\sqrt{\text{Var}(v)\text{Var}(v_a)}} \tag{14}$$

where v & v_a represent the noisy and despeckled signals, respectively, Cov() calculates the covariance, and Var() calculates the variance.

First, the simulated signal $v_1(t)$ with SNR $= -10$ dB is processed by the despeckling algorithm in section 2. Figure 6(a)

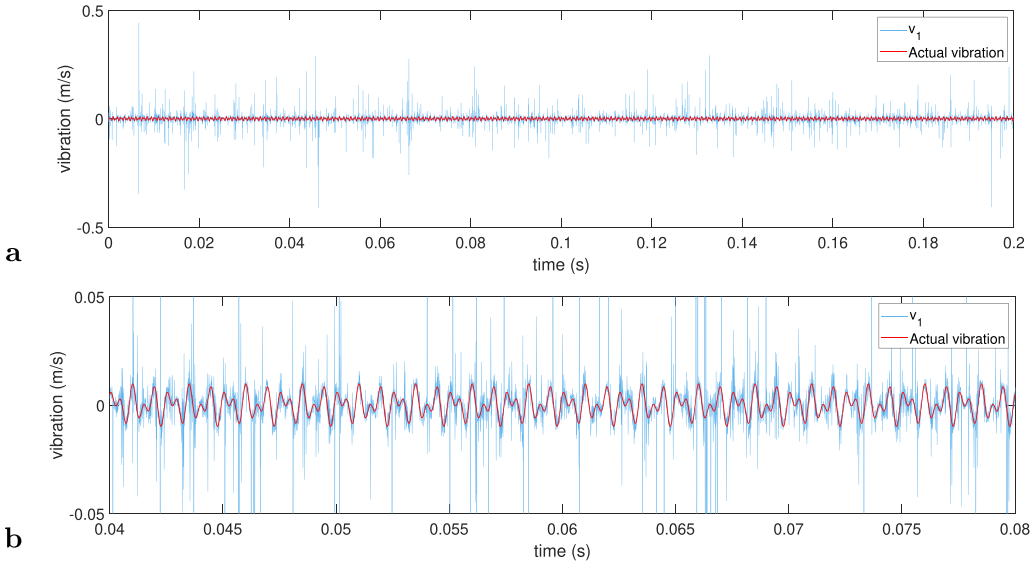

Figure 3. (a) $v_1(t)$ with SNR $= -10$ dB; (b) magnified signal of (a).

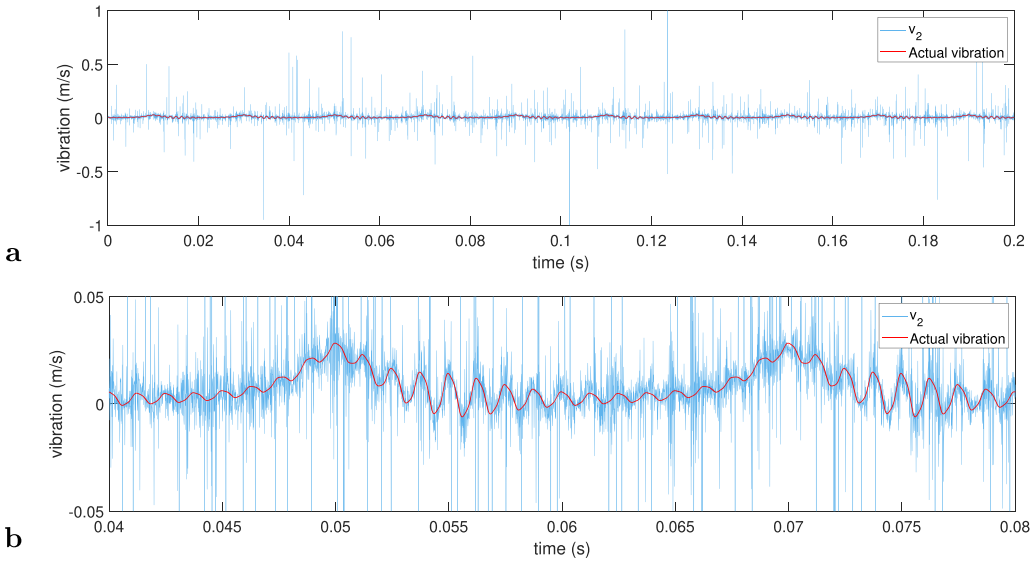

Figure 4. (a) $v_2(t)$ with SNR $= -10$ dB; (b) magnified signal of (a).

presents the MRMS thresholds, which cut off the signal dropouts but preserve the dominant speckle-noise energy, and we get the cut-off signal $v_1'(t)$. Using $v_1'(t)$ minus the summation of IMF1 to IMF7 (figure 6(b)), the remaining component agrees well with the actual vibration, as shown in figure 7(a). The post SNR increases to 12.48 dB, and the correlation coefficient is $\delta = 0.9728$, which means that the processed signal is almost the same as the true vibration. However, the BPF and DWT methods fail to achieve comparable results, as numerous visible distortions remain in figures 7(b) and (c). We use the cut-off frequency of 600 Hz for the BPF and 4 frequency bands for the DWT with 'db4' wavelets. These choices are best in our trials but not the optimized one. The post SNRs of the BPF and DWT results are 5.53 dB and 0.23 dB, respectively, while their correlation coefficients are only 0.8597 and 0.7478.

Second, the simulated signals $v_2(t)$ & $v_3(t)$ are processed to remove speckle noise, with the results presented in figure 8. The EEMD-based approach effectively eliminates the speckle noise, as shown in figures 8(a) and (b). The post SNRs increase to 18.71 dB for the signal $v_2(t)$ and 25.69 dB for the signal $v_3(t)$, and their correlation coefficients are 0.9872 and 0.9868, respectively. However, the BPF and DWT approaches preserve numerous distortions. Both their post SNRs and correlation coefficients are far lower than those of the EEMD-based results (seen in table 2). Therefore, our proposed algorithm demonstrates advantages in removing speckle noise.

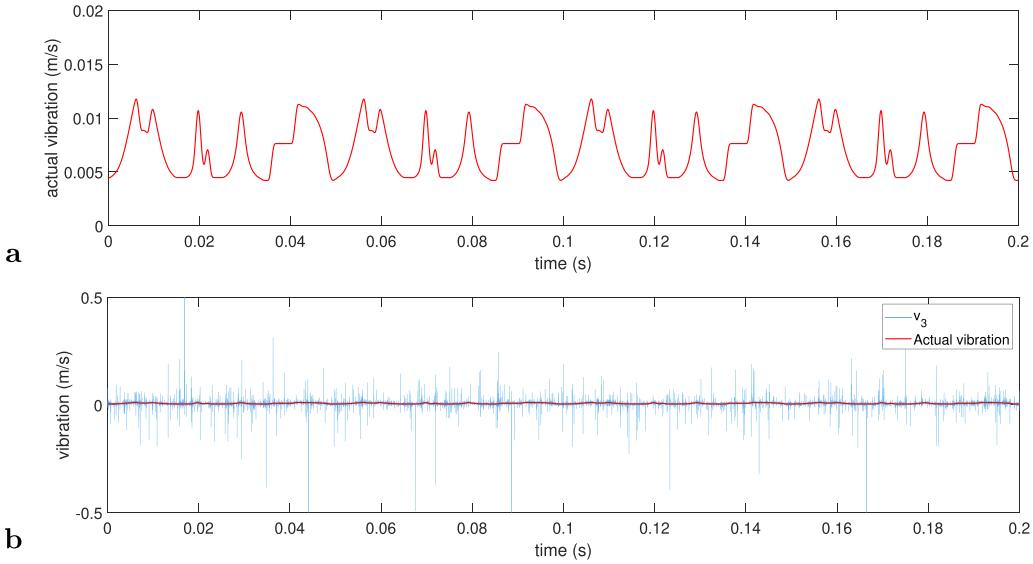

Figure 5. (a) The actual vibration $v_{3a}(t)$; (b) $v_3(t)$ with SNR $= -10$ dB.

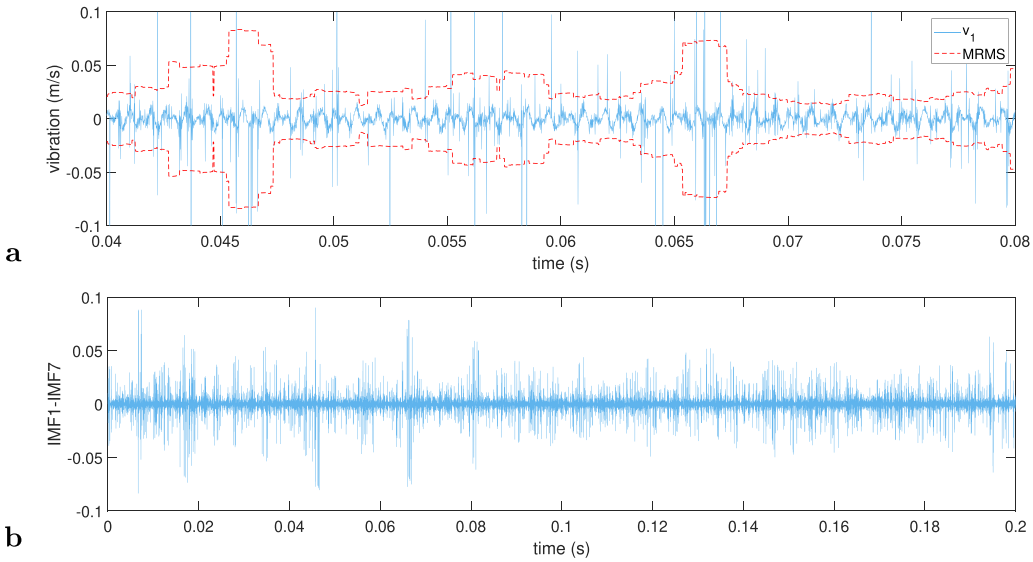

Figure 6. (a) The MRMS thresholds of $v_1(t)$ (magnified signal); (b) the summation of IMF1 to IMF7.

To evaluate the robustness of the EEMD-based approach, we modify the initial SNRs, with the results shown in table 2. Generally, all three approaches perform better with increasing initial SNR. When the initial SNR is -5 dB, the proposed approach outperforms the others, although the BPF and DWT achieve acceptable despeckling results (with correlation coefficients over 0.89). When the initial SNR decreases to -15 dB, the BPF and DWT methods fail to eliminate speckle noise with correlation coefficients below 0.71. Nonetheless, the EEMD-based approach achieves correlation coefficients over 0.93, which means that the processed signals are almost the same as the true vibrations. These promising results regardless of the noise intensity indicate the advantages and robustness of our developed method.

4. Experimental investigation

4.1. First scenario

First, we use a small-scale setup to evaluate the despeckling approach for LDVom measurements. Although the setup is similar to some SLDV and CSLDV research (e.g. [20]), the conditions of using the LDVom are held: one-way scanning and unable to enhance the surface reflection. Figure 9 illustrates its schematic, and the experimental setup with multiple instruments is presented in figure 10. An artificially excited steel strip with defected surface is monitored by the LDVom. This steel strip (length 540 mm) has three artificial defects (with a profile of 6×4 mm at different locations 40 mm,

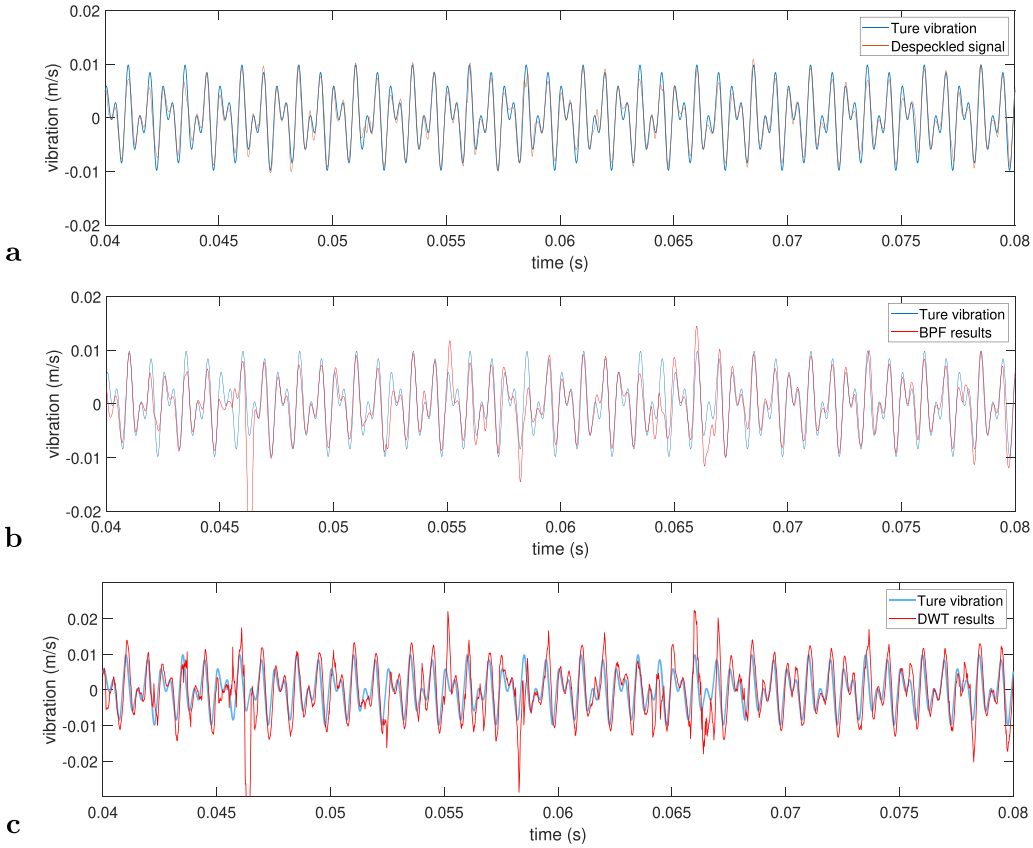

Figure 7. The despeckling results of (a) the proposed approach, (b) BPF, and (c) DWT. The signals are magnified between 0.04 s and 0.08 s.

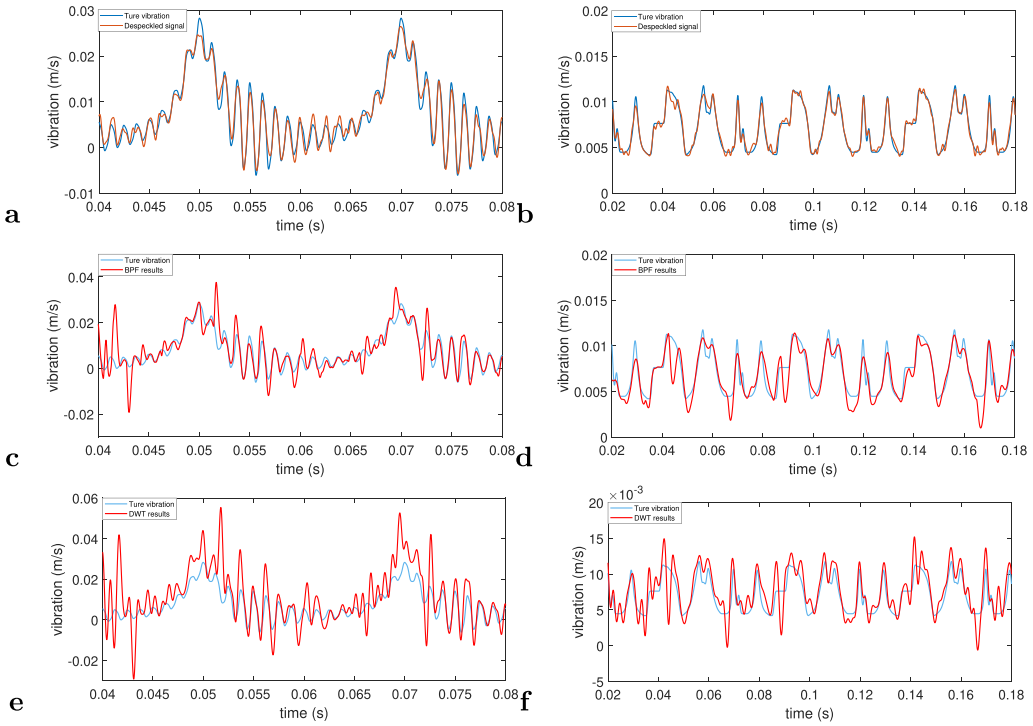

Figure 8. The despeckling results for (a) $v_2(t)$ by the proposed approach, (b) $v_3(t)$ by the proposed approach, (c) $v_2(t)$ by the BPF, (d) $v_3(t)$ by the BPF, (e) $v_2(t)$ by the DWT, and (f) $v_3(t)$ by the DWT. The signals have been magnified.

Table 2. Post SNRs and correlation coefficients of the despeckling results.

$v_1(t)$ initial SNR		−10 dB	−5 dB	−15 dB
Proposed approach	Post SNR	12.48 dB	13.11 dB	8.87 dB
	Correlation	0.9728	0.9754	0.9403
BPF	Post SNR	5.53 dB	9.41 dB	0.96 dB
	Correlation	0.8597	0.9413	0.6887
DWT	Post SNR	0.23 dB	9.71 dB	−0.30 dB
	Correlation	0.7478	0.9488	0.6709
$v_2(t)$ initial SNR		−10 dB	−5 dB	−15 dB
Proposed approach	Post SNR	18.71 dB	22.61 dB	15.21 dB
	Correlation	0.9872	0.9947	0.9708
BPF	Post SNR	6.97 dB	12.55 dB	2.78 dB
	Correlation	0.8481	0.9492	0.7069
DWT	Post SNR	4.50 dB	9.66 dB	0.44 dB
	Correlation	0.8169	0.9382	0.6613
$v_3(t)$ initial SNR		−10 dB	−5 dB	−15 dB
Proposed approach	Post SNR	25.69 dB	30.33 dB	18.99 dB
	Correlation	0.9868	0.9954	0.9350
BPF	Post SNR	13.86 dB	17.98 dB	9.14 dB
	Correlation	0.8100	0.9176	0.6023
DWT	Post SNR	9.91 dB	16.28 dB	6.29 dB
	Correlation	0.7418	0.8972	0.5131

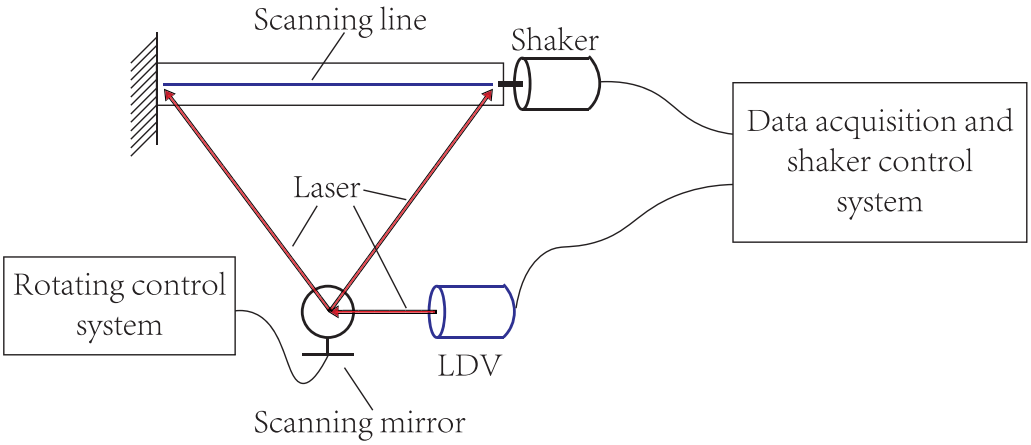

Figure 9. A schematic of an LDVom scanning a beam.

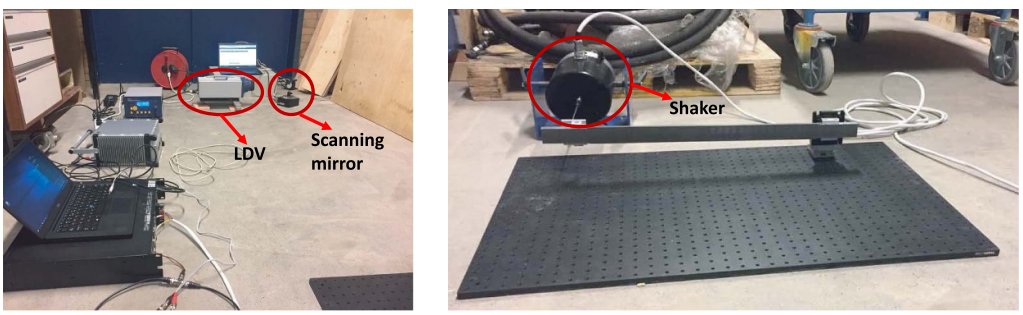

Figure 10. Experimental setup for scanning the steel strip.

Figure 11. Steel strip with three artificial defects.

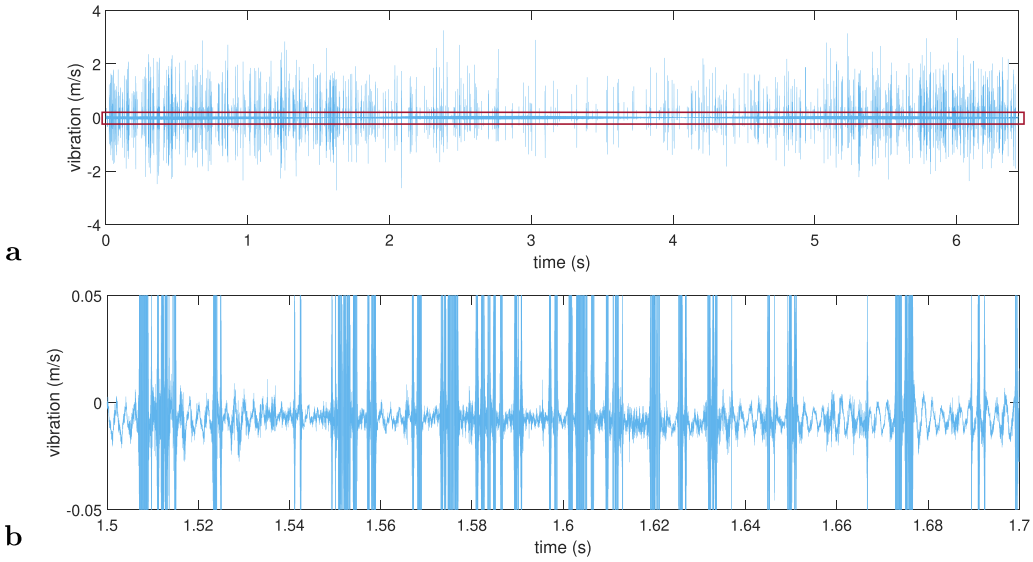

Figure 12. (a) The original signal; (b) magnified signal between 1.5 s and 1.7 s.

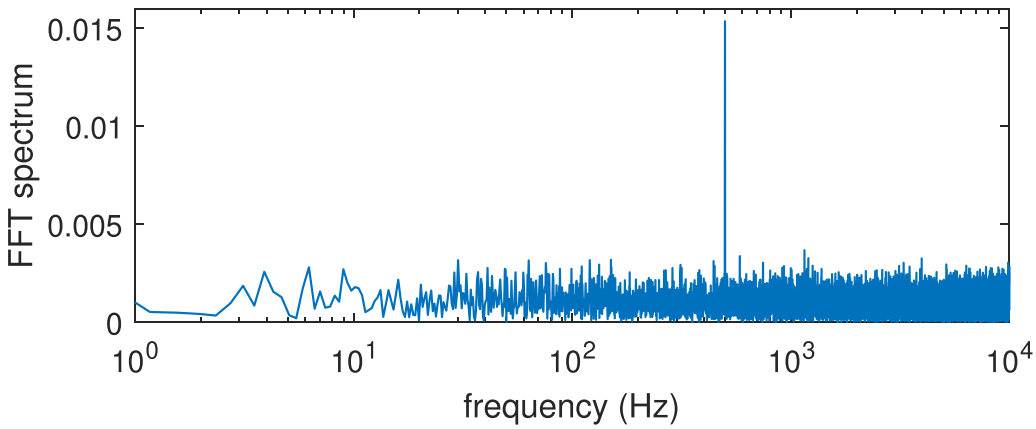

Figure 13. The FFT spectrum of the original signal.

220 mm, and 450 mm) through the strip width, as shown in figure 11. We firmly mount the steel strip as a cantilever beam over the base. The left end of the strip is excited by a shaker with a 500 Hz sinusoidal wave. During the scanning progress, the rotating mirror first deflects the transmission laser beam onto the left end and then scans the strip surface at a constant speed around 0.85 m s^{-1}. The sampling frequency is 102 400 Hz. A high sampling frequency is chosen to avoid mixing the vibration frequency with the signal drop-outs. If the sampling frequency is low, the signal drop-outs will appear in low-frequency bands and make the vibration confusing. The LDV used is 'RSV-150' made by 'Polytec' and the measurement resolution used is 100 mm s^{-1} V^{-1}. It should be noticed that adjusting the measurement range cannot change speckle noise, since the noise is produced by the laser but not by the instrument units [10].

Figure 12 shows the original vibration signal acquired by the LDVom. The speckle noise is extremely intense as the actual vibration (marked inside the red rectangle) is nearly invisible. The amplitudes of the signal drop-outs reach approximately 3 m s^{-1}, over 60 times the true vibration at approximately 500 Hz. Figure 12(b) presents the magnified signal between 1.5 s and 1.7 s. The speckle noise covers numerous local oscillations, increasing difficulties in local modal analysis. The fast Fourier transform (FFT) spectrum of the original signal is presented in figure 13, which also shows the

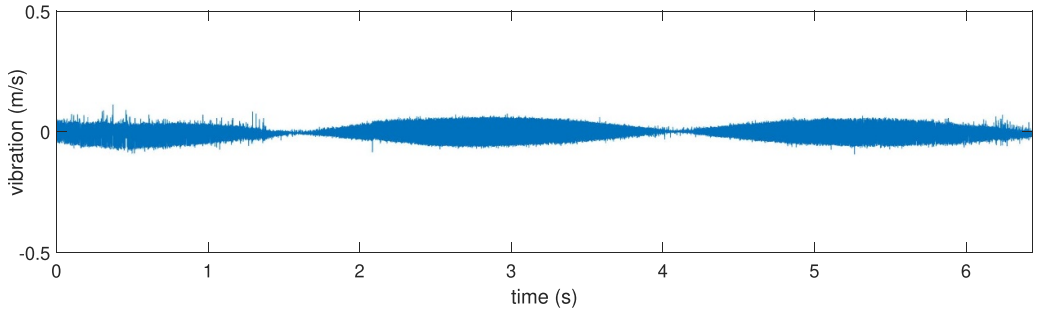

Figure 14. The despeckled signal obtained by the proposed EEMD-based approach.

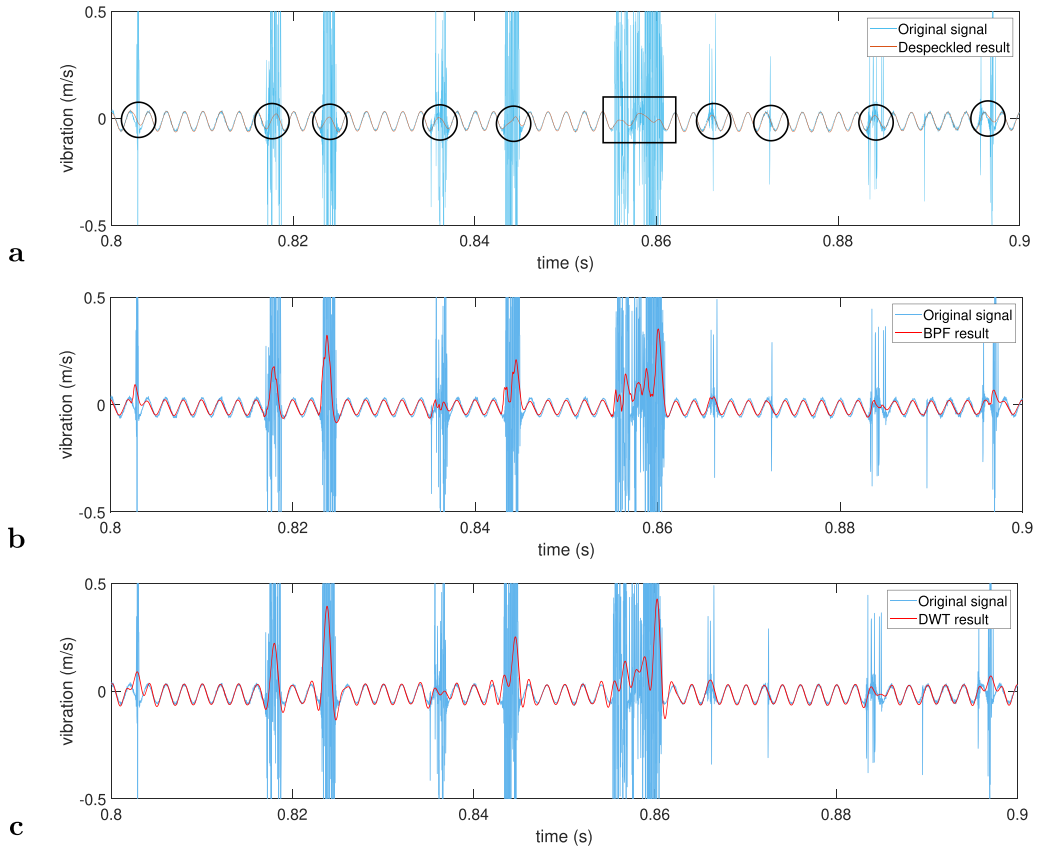

Figure 15. The despeckling results of (a) the proposed approach, (b) BPF, and (c) DWT. Signals are magnified between 0.8 s and 0.9 s.

vibration frequency is 500 Hz. Since the LDVom measurement is one-way, the spectrum has no sideband harmonics that appear in CSLDV signal spectrum.

Since the EEMD-based approach is time- and memory-consuming in processing complicated signals, we divide the data into multiple 0.1 s time series to remove the speckle noise and then merge the processed series. With IMF1 to IMF8 discarded, the despeckling results are presented in figure 14. The vibration amplitudes are recovered to normal levels, and the energy distribution becomes visible. The initial SNR is estimated to be −14.63 dB by regarding the despeckled signal as the actual vibrations. This also means the speckle noise is extremely intense, similar to the simulated cases in section 3.

Figure 15 shows the magnified despeckled signal between 0.8 s and 0.9 s. The developed approach reveals the true vibration surrounding 500 Hz, especially from oscillations polluted by intense speckle noise (marked with black circles). At the locations covered by continuously intense speckle noise (marked with a black rectangle), the processed results approximately recover the true waveforms. However, speckle noise significantly distorts the BPF and DWT results, especially at approximately 0.86 s.

Figure 16 shows the magnified despeckled signal where the initial SNR is estimated to be −27.79 dB and the actual vibration amplitudes are 1/5 to 1/10 of those in figure 15. Although the vibration responses are extremely weak, signals covered by intense noise (marked with a black rectangle)

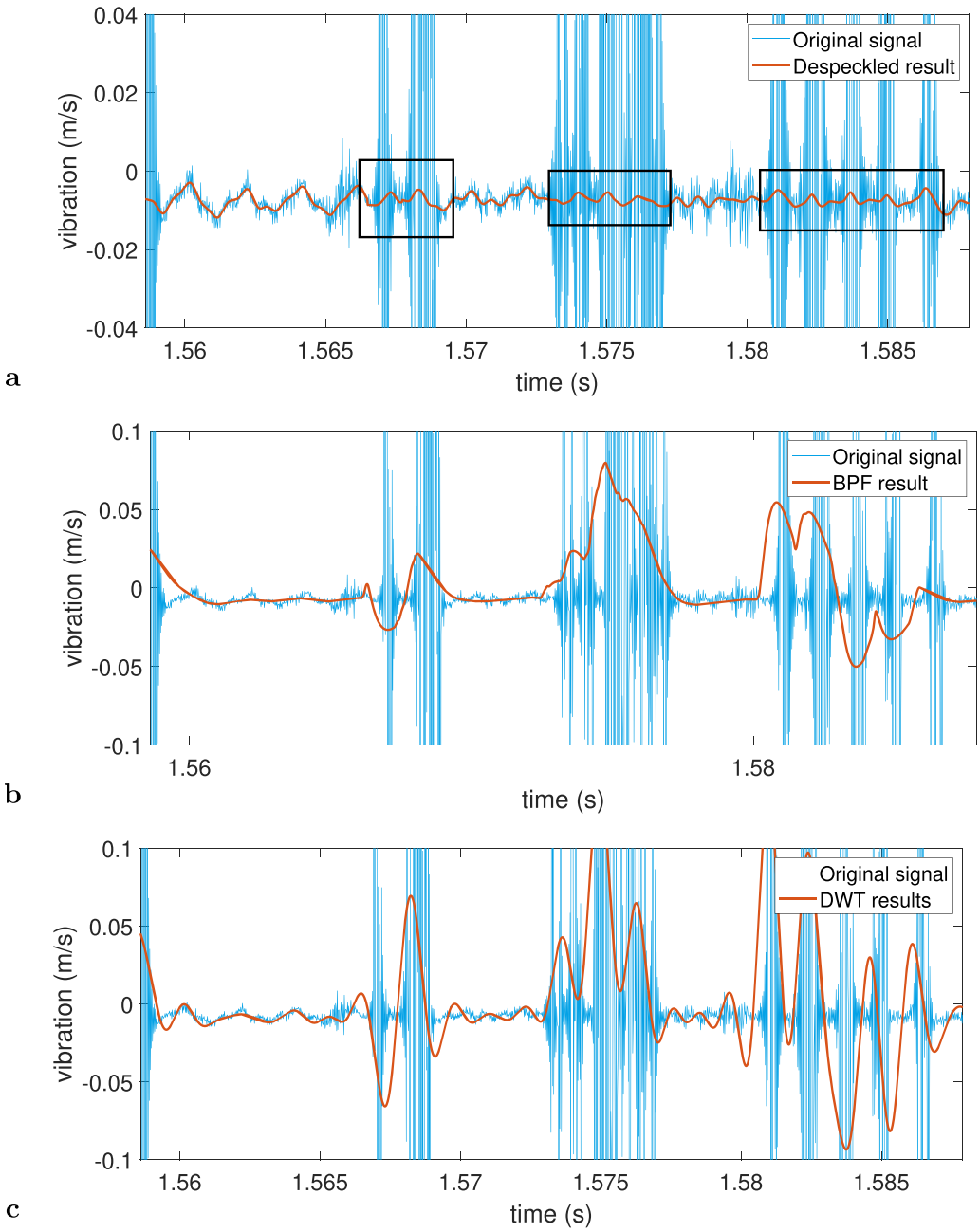

Figure 16. The despeckling results of (a) the proposed approach, (b) BPF, and (c) DWT. The signal segment with an estimated SNR of −27.79 dB is magnified.

are approximately revealed. However, the results of BPF and DWT are unpromising, containing significant distortions at intense speckle locations. Therefore, the developed EEMD-based approach demonstrates advantages in processing signals to eliminate speckle noise.

For further vibration analysis and damage inspection, the Hilbert–Huang spectrum has potential for signal interpretation, as illustrated in figure 17. The despeckled signal in figure 14 contains three bulbous segments corresponding to three defects. In the Hilbert spectrum, the signal frequency varies around the central frequency of 500 Hz. The actual vibration is not an absolute sinusoidal wave, thus causing instantaneous variant frequencies. It is noticeable that the vibration energy at the defect locations is larger than that in other areas. Therefore, we identify the local maximum energy locations as defect locations. In this case, we estimate defect centers at 0.4931 s, 2.748 s and 5.477 s from the Hilbert–Huang spectrum, corresponding to 41.4 mm, 230.6 mm and 459.7 mm. Thus, the Hilbert–Huang spectrum can reveal the damage locations from the despeckled signal despite approximately 1 cm errors.

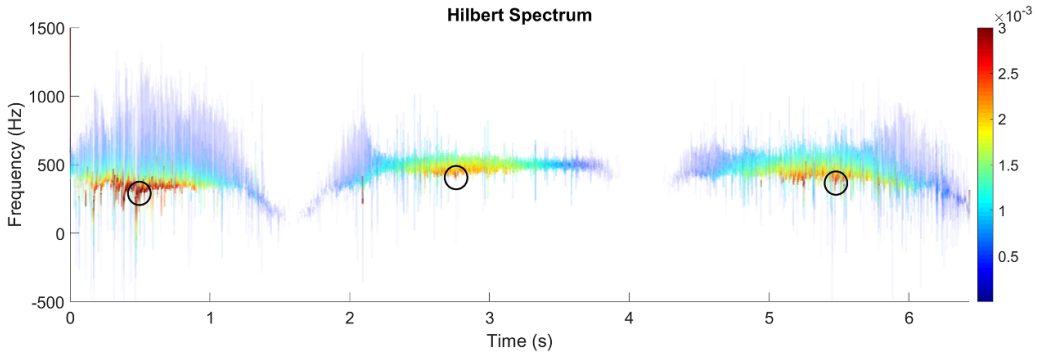

Figure 17. The Hilbert–Huang spectrum of the despeckled signal.

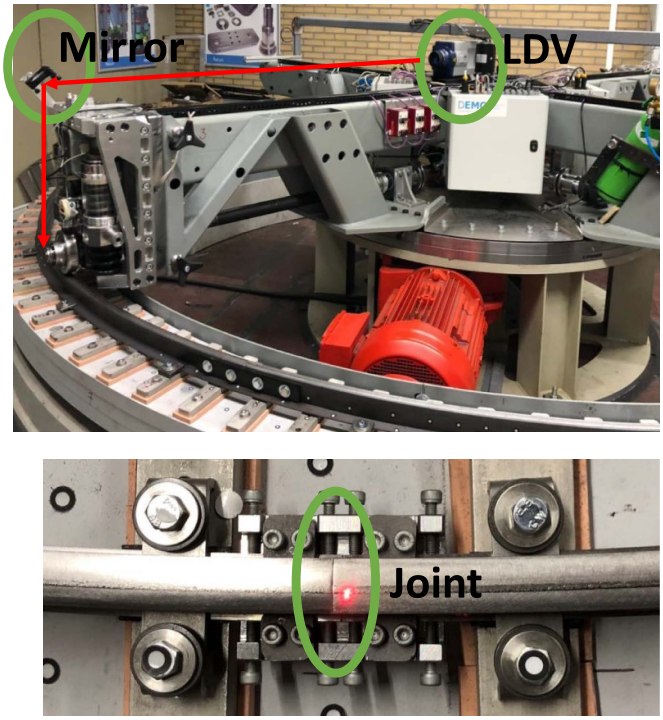

Figure 18. The experimental setup of the running railway system.

4.2. Second scenario

Second, we mount the LDVom on a downscaled running railway system [45] (as shown in figure 18) to acquire the vibrations excited by wheel-rail contact. The laser is deflected by a fixed mirror to focus on the rail surface. With the running system, the LDVom continuously scans the rail surface. The running speed is 10 km h^{-1} and the sampling frequency is 102 400 Hz.

Here, we take the signal segment when the wheel passes the joint for analysis, with the signal illustrated in figure 19. The noise is intense with frequent signal drop-outs to cover the vibrations. Therefore, the waveform when wheel hits the joint (marked with the blue circle) becomes indistinguishable in the original signal. Using the EEMD-based approach and discarding the first eight IMFs, the depseckled signal has revealed the trend of the original one, as shown in figure 19(a). The despeckling process does not change or mitigate the vibration modes, as the vibration frequency peaks (marked in the black circles) in FFT spectra (figure 20) remains invariant between original and despeckling signals. These frequency peaks are not related to the speckle noise since the measurement is not cyclical. The dominant noise energy has attenuates sharply (marked in the red circle). However, the EEMD-based approach is different from a low-pass filter, as the low-frequency energy (which may related to speckle noise) also alters (e.g. marked in the red rectangle).

The waveform at the joint location becomes visible, and we can also use an IMF to locate the joint, e.g. IMF10. As illustrated in figure 19(b), the IMF10 presents a sharp amplitude at around 0.225 s, corresponding to the wheel hitting the joint. The amplitude of an IMF is corresponding to the operating deflection shape, and thus can be used for vibration analysis. Hilbert–Huang spectrum also has potential for vibration

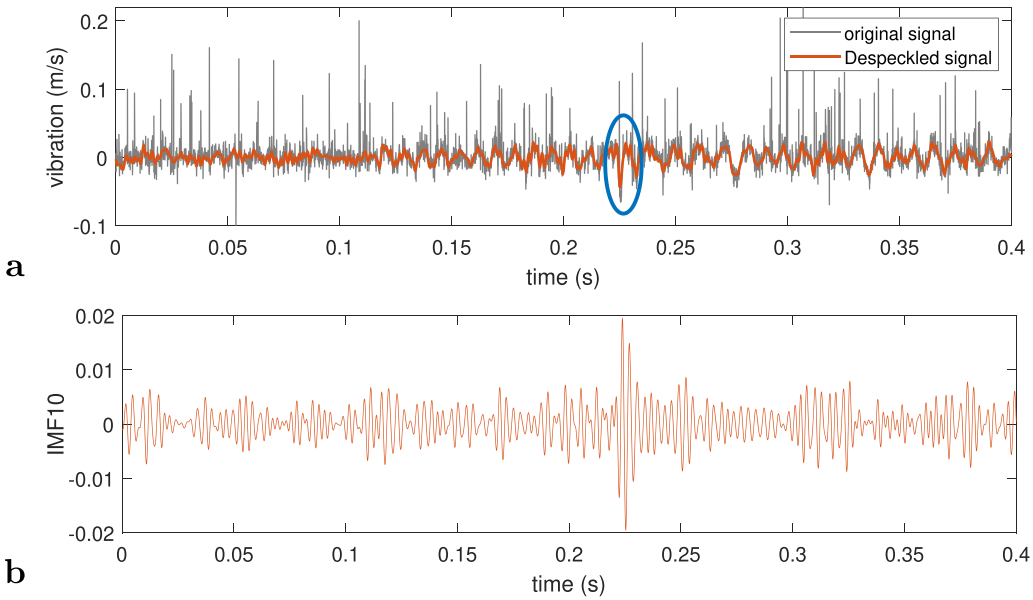

Figure 19. (a) The original and the despeckled signals when the wheel passing the joint; (b) the IMF10 achieved by EEMD.

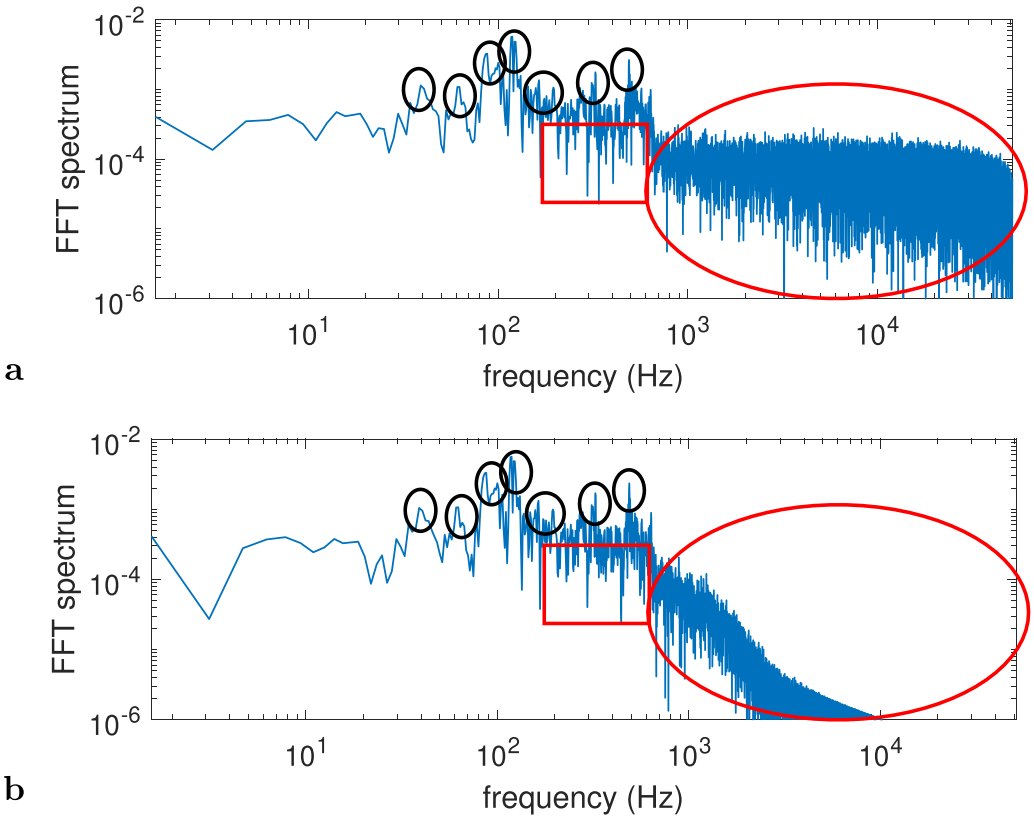

Figure 20. The FFT spectra of (a) the original signal and (b) the despeckled signal.

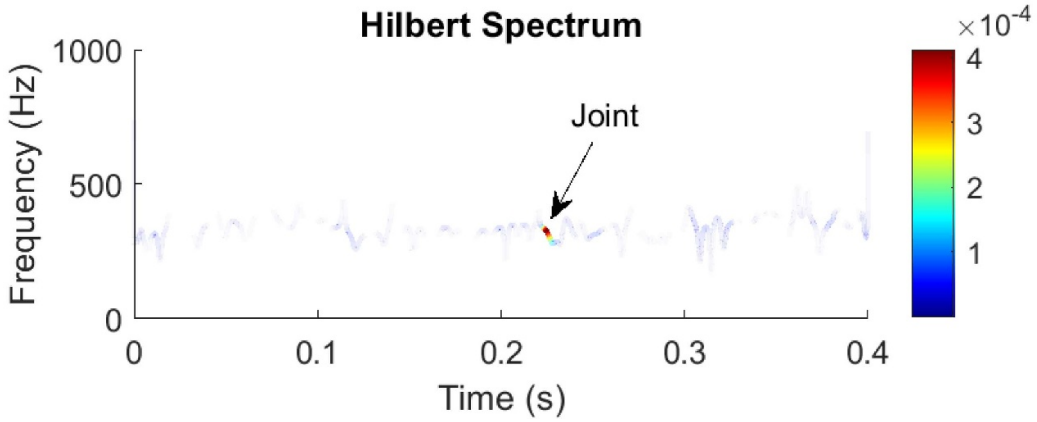

Figure 21. The Hilbert–Huang spectrum of the IMF10.

analysis, with that of IMF10 shown in figure 21. Only one spike energy appears around 0.225 s, agreeing well with the joint location. Therefore, our proposed approach can eliminate the speckle noise and reveal the signals for vibration analysis.

5. Conclusion and discussions

In this paper, we propose an EEMD-based approach for eliminating speckle noise in LDVom signals. LDVom is a one-way continuously scanning technique especially used for large-scale structural monitoring, e.g. railway tracks, different from SLDV and CSLDV. Speckle noise, originating from phase variation of speckle patterns, is a significant issue when scanning from moving platforms. The noise amplitudes can exceed 30 times the true vibration, and the SNR can drop below −15 dB. The EEMD approach can acquire IMFs containing the instantaneous frequency, which relates to the instantaneous vibration velocity captured by the LDVom. The related Hilbert–Huang spectrum has the potential to highlight the damage locations. Since the instantaneous frequency in an IMF is continuous, the EEMD approach can restore the actual oscillations affected by intense speckle noise. MRMS thresholds are used for cutting off the outliers, which can reduce drop-out amplitudes and generate noise discontinuities that EEMD can identify properly. The proposed method is evaluated regarding processing numerically simulated and experimental acquired signals.

In the numerical simulation, randomly generated speckle noise is added to three different time series, including a stationary signal, a time-varying signal and an abnormal signal with oscillation discontinuities. When the initial SNR is −10 dB, our proposed approach can reveal the true vibrations, with post SNRs = 12.48 dB, 18.71 dB & 25.69 dB and correlation coefficients over 0.97. The BPF and DWT methods for comparison remove only part of the speckle noise and reserve numerous distortions. Generally, all three approaches perform better with increasing initial SNR. The EEMD-based approach can achieve promising results even with initial SNR = −15 dB, and the correlation coefficients remain over 0.93. However, the BPF and DWT results are unacceptable in such intensely noisy situations. Therefore, these results indicate the advantages and robustness of our proposed approach in eliminating speckle noise.

In the first physical experiment, a steel strip with three artificial defects is excited at 500 Hz. The speckle noise is intense as the noise amplitudes can reach 35 times the vibrations, and the estimated initial SNR is −14.63 dB. After IMF1 to IMF8 are discarded, the actual vibration is revealed with energy concentrating on the defect locations. Generally, the EEMD-based approach can restore the vibrations surrounding 500 Hz regardless of the speckle intensities, even at the locations where the actual vibrations are extremely weak and the initial SNR is estimated to be −27.79 dB. However, both the BPF and DWT methods preserve amplitude distortions resulting from intense speckle noise. The Hilbert–Huang spectrum is illustrated to identify defect centers. The estimated damage locations are at 41.4 mm, 230.6 mm and 459.7 mm, corresponding well with the actual locations of 40 mm, 220 mm and 450 mm.

In the second physical experiment, a downscaled running railway system excited by wheel-rail contact is under detection. The speckle noise is intense to cover the vibration, especially the waveform at the joint location. The proposed approach successfully mitigates the speckle noise. The joint location is identified in both an IMF and the Hilbert–Huang spectrum. Therefore, our proposed approach is applicable to eliminating speckle noise and the despeckled signal can be used for damage inspection.

We want to mention that the simulated signals are much more challenging than the experimental signal of 500 Hz, and we want to evaluate the effect on these challenging signals. That is reason for the difference between the simulated ones and the experimental ones. Besides, the despeckling effect seems more visible in removing the signal drop-outs, which is a specific characteristic within the speckle noise resulting from large phase change. It is difficult to visibly evaluate the effect on other frequencies, and therefore we use 'signal-to-noise ratio' to evaluate the despeckling effect.

There are two issues when applying EEMD, which should be investigated in future research. First, EEMD has increased the computational burden since it repeats EMD several

hundred times. This issue may be solved by paralleling computation for the hundred times of EMD. Second, the choice of IMFs for despeckled signals is dependent on the operating experience. Future research will develop automatic approaches to distinguish between the IMFs for noise and vibration.

Future research should also concern the despeckling effect in different scenarios. The experimental parameters like the vibration frequency, the sampling frequency and the scanning speed would change the signals, and the despeckling effect that changes with these parameters should be further investigated. Besides, the despeckling effect on the impulsive signal is unknown, which should also be investigated in the future research.

We also want to mention that using Hilbert–Huang transform is potential for vibration analysis. However, different strategies can present different analyzing effects. Since the issue of signal quality has been solved, the strategies to interpret LDVom signals can be developed in future research.

Data availability statement

The data that support the findings of this study are available upon reasonable request from the authors.

ORCID iD

Yang Jin https://orcid.org/0000-0003-1613-3898

References

[1] Mazzù A, Provezza L, Zani N, Petrogalli C, Ghidini A and Faccoli M 2019 Effect of shoe braking on wear and fatigue damage of various railway wheel steels for high speed applications *Wear* **434–435** 203005
[2] Wang K, Tan Z, Gu K, Gao B, Gao G, Misra R and Bai B 2017 Effect of deep cryogenic treatment on structure-property relationship in an ultrahigh strength Mn-Si-Cr bainite/martensite multiphase rail steel *Mater. Sci. Eng.* A **684** 559–66
[3] Magel E and Kalousek J 2017 Designing and assessing wheel/rail profiles for improved rolling contact fatigue and wear performance *Proc. Inst. Mech. Eng.* F **231** 805–18
[4] Magel E, Mutton P, Ekberg A and Kapoor A 2016 Rolling contact fatigue, wear and broken rail derailments *Wear* **366–367** 249–57
[5] Salawu O 1997 Detection of structural damage through changes in frequency: a review *Eng. Struct.* **19** 718–23
[6] Hou R, Xia Y and Zhou X 2018 Structural damage detection based on l1 regularization using natural frequencies and mode shapes *Struct. Control Health Monit.* **25** e2107
[7] Zhou C, Hong M, Su Z, Wang Q and Cheng L 2013 Evaluation of fatigue cracks using nonlinearities of acousto-ultrasonic waves acquired by an active sensor network *Smart Mater. Struct.* **22** 015018
[8] Khairi M T M, Ibrahim S, Yunus M A M, Faramarzi M, Sean G P, Pusppanathan J and Abid A 2019 Ultrasound computed tomography for material inspection: principles, design and applications *Measurement* **146** 490–523
[9] Stanbridge A and Ewins D 1999 Modal testing using a scanning laser Doppler vibrometer *Mech. Syst. Signal Process.* **13** 255–70
[10] Rothberg S *et al* 2017 An international review of laser Doppler vibrometry: making light work of vibration measurement *Opt. Lasers Eng.* **99** 11–22
[11] Siringoringo D M and Fujino Y 2006 Experimental study of laser Doppler vibrometer and ambient vibration for vibration-based damage detection *Eng. Struct.* **28** 1803–15
[12] Chen D-M, Xu Y and Zhu W 2018 Non-model-based multiple damage identification of beams by a continuously scanning laser Doppler vibrometer system *Measurement* **115** 185–96
[13] Martarelli M and Ewins D J 2006 Continuous scanning laser Doppler vibrometry and speckle noise occurrence *Mech. Syst. Signal Process.* **20** 2277–89
[14] Nishizawa O, Satoh T, Lei X and Kuwahara Y 1997 Laboratory studies of seismic wave propagation in inhomogeneous media using a laser Doppler vibrometer *Bull. Seismol. Soc. Am.* **87** 809–23
[15] Sriram P, Craig J and Hanagud S 1990 A scanning laser Doppler vibrometer for modal testing *Int. J. Anal. Exp. Modal Anal.* **5** 155–67
[16] Stanbridge A and Ewins D 1996 Measurement of translational and angular vibration using a scanning laser Doppler vibrometer *Shock Vib.* **3** 141–52
[17] Akamatsu R, Sugimoto T, Utagawa N and Katakura K 2013 Proposal of non contact inspection method for concrete structures using high-power directional sound source and scanning laser Doppler vibrometer *Jpn. J. Appl. Phys.* **52** 07HC12
[18] Liu C, Zang C and Zhou B 2020 A novel algorithm for determining the pose of a scanning laser Doppler vibrometer *Meas. Sci. Technol.* **31** 025202
[19] Allen M S and Sracic M W 2010 A new method for processing impact excited continuous-scan laser Doppler vibrometer measurements *Mech. Syst. Signal Process.* **24** 721–35
[20] Xu Y, Chen D-M and Zhu W 2017 Damage identification of beam structures using free response shapes obtained by use of a continuously scanning laser Doppler vibrometer system *Mech. Syst. Signal Process.* **92** 226–47
[21] Chen D-M, Xu Y and Zhu W 2018 Identification of damage in plates using full-field measurement with a continuously scanning laser Doppler vibrometer system *J. Sound Vib.* **422** 542–67
[22] Huang Z and Zang C 2020 Fast modal rotation measurement using a dual sinusoidal-scan continuously scanning laser Doppler vibrometer *Meas. Sci. Technol.* **31** 085201
[23] Di Maio D, Castellini P, Martarelli M, Rothberg S, Allen M, Zhu W and Ewins D 2021 Continuous scanning laser vibrometry: a raison d'être and applications to vibration measurements *Mech. Syst. Signal Process.* **156** 107573
[24] Rahimi S, Li Z and Dollevoet R 2014 Measuring with laser Doppler vibrometer on moving frame (LDVMF) *AIP Conf. Proc.* **1600** 274–86
[25] Martin P and Rothberg S 2009 Introducing speckle noise maps for laser vibrometry *Opt. Lasers Eng.* **47** 431–42
[26] Goodman J W 1963 Statistical properties of laser sparkle patterns *Technical Report* (Stanford University CA Stanford Electronics Labs)
[27] Rothberg S 2006 Numerical simulation of speckle noise in laser vibrometry *Appl. Opt.* **45** 4523–33
[28] Chiariotti P, Martarelli M and Revel G 2017 Delamination detection by multi-level wavelet processing of continuous scanning laser Doppler vibrometry data *Opt. Lasers Eng.* **99** 66–79
[29] Zhu J, Li Y and Baets R 2019 Mitigation of speckle noise in laser Doppler vibrometry by using a scanning average method *Opt. Lett.* **44** 1860–3
[30] Xu Y, Chen D-M and Zhu W 2020 Modal parameter estimation using free response measured by a continuously scanning laser Doppler vibrometer system with application to structural damage identification *J. Sound Vib.* **485** 115536

[31] Jin Y and Li Z 2021 Eliminating speckle noises for laser doppler vibrometer based on empirical wavelet transform *2021 13th Int. Conf. on Measurement* (IEEE) pp 72–75
[32] Huang N E, Shen Z, Long S R, Wu M C, Shih H H, Zheng Q, Yen N-C, Tung C C and Liu H H 1998 The empirical mode decomposition and the Hilbert spectrum for nonlinear and non-stationary time series analysis *Proc. R. Soc.* A **454** 903–95
[33] Feng Z, Liang M, Zhang Y and Hou S 2012 Fault diagnosis for wind turbine planetary gearboxes via demodulation analysis based on ensemble empirical mode decomposition and energy separation *Renew. Energy* **47** 112–26
[34] OBrien E J, Malekjafarian A and González A 2017 Application of empirical mode decomposition to drive-by bridge damage detection *Eur. J. Mech.* A **61** 151–63
[35] Tian P, Cao X, Liang J, Zhang L, Yi N, Wang L and Cheng X 2014 Improved empirical mode decomposition based denoising method for lidar signals *Opt. Commun.* **325** 54–59
[36] Rakshit M and Das S 2018 An efficient ECG denoising methodology using empirical mode decomposition and adaptive switching mean filter *Biomed. Signal Process. Control* **40** 140–8
[37] Gómez J L and Velis D R 2016 A simple method inspired by empirical mode decomposition for denoising seismic data *Geophysics* **81** V403–13
[38] Wu Z and Huang N E 2009 Ensemble empirical mode decomposition: a noise-assisted data analysis method *Adv. Adap. Data Anal.* **1** 1–41
[39] Rothberg S, Baker J and Halliwell N 1989 Laser vibrometry: pseudo-vibrations *J. Sound Vib.* **135** 516–22
[40] Halliwell N A 1993 Laser vibrometry *Optical Methods in Engineering Metrology* (Berlin: Springer) pp 179–211
[41] Hou T Y and Shi Z 2011 Adaptive data analysis via sparse time-frequency representation *Adv. Adapt. Data Anal.* **3** 1–28
[42] Mert A and Akan A 2014 Detrended fluctuation thresholding for empirical mode decomposition based denoising *Digit. Signal Process.* **32** 48–56
[43] Rader C M and Gold B 1967 Digital filter design techniques in the frequency domain *Proc. IEEE* **55** 149–71
[44] Edwards T 1991 Discrete wavelet transforms: theory and implementation *Universidad de* 28–35
[45] Naeimi M, Li Z, Petrov R H, Sietsma J and Dollevoet R 2018 Development of a new downscale setup for wheel-rail contact experiments under impact loading conditions *Exp. Tech.* **42** 1–17